Journal of Photochemistry and Photobiology A: Chemistry 203 (2009) 166–176

Contents lists available at ScienceDirect

Journal of Photochemistry and Photobiology A: Chemistry

journal homepage: www.elsevier.com/locate/jphotochem

Intramolecular interactions and photoinduced electron transfer in isoalloxazine-naphthalene bichromophores

Gianluca Accorsi[a,1], Francesco Barigelletti[a], Angeles Farrán[b,2], Fernando Herranz[b,2], Rosa María Claramunt[b,2], Massimo Marcaccio[c,3], Giovanni Valenti[c,3], Francesco Paolucci[c,*], Elena Pinilla[d,4], María Rosario Torres[d,4]

[a] Istituto per la Sintesi e la Fotoreattivitá (ISOF), Consiglio Nazionale delle Ricerche (CNR), Via Gobetti 101, Bologna, Italy
[b] Departamento de Química Orgánica y Bio-Orgánica, Facultad de Ciencias, Universidad Nacional de Educación a Distancia (UNED), Paseo Senda del Rey 9, 28040 Madrid, Spain
[c] SuprEMat, Dipartimento di Chimica G. Ciamician, Alma Mater Studiorum Università di Bologna, Via Selmi 2, Bologna, Italy
[d] Departamento de Química Inorgánica I, Laboratorio de Rayos X, Facultad de Ciencias Químicas, Universidad Complutense de Madrid (UCM), Madrid, Spain

ARTICLE INFO

Article history:
Received 3 December 2008
Received in revised form 10 January 2009
Accepted 14 January 2009
Available online 30 January 2009

This paper is dedicated to Prof. D.C. Neckers on his 70th birthday.

Keywords:
Flavine
Macrocycles
Photochemistry
Electrochemistry
Electron transfer

ABSTRACT

The synthesis, the structural characterization and electrochemical and photophysical properties of new linear (**OFn**) and macrocyclic (**MFn**) bichromophoric systems containing one flavin and one naphthalene moiety, separated by $(CH_2)_n$ alkyl chains ($n = 4$ or 6), are reported. The electrochemical properties of **OF4**, **OF6**, **MF4**, **MF6** were investigated by cyclic voltammetry (CV) in ultra-dry THF and compared with the model compounds containing either the flavin unit (**FL6**) or the monomethoxy- (**mona**) and dimethoxy naphthalene (**dmona**) derivatives, respectively. While only minor ground-state interactions were evidenced between the chromophores in the voltammetric curves and absorption spectra of bichromophores, luminescence data evidenced intramolecular photoinduced electron transfer processes as main deactivation routes of flavin-centered excited states. The rates of the intramolecular photoinduced electron transfer, involving the oxynaphthalene moieties as electron donors, were finally determined.

1. Introduction

Flavoenzymes are among the structurally and functionally most diverse family of redox proteins [1–3]. They are involved in a wide range of biotransformations ranging from Baeyer-Villiger oxidations to aromatic hydroxylations and DNA photorepair. Their functionality is associated to a single redox unit, either the FMN (flavin mononucleotide) or FAD (flavin adenine dinucleotide) which is incorporated into the proteic structure either non-covalently or covalently, linked to a peptide fragment via the C8 of the isoalloxazine ring.

The redox events take place stepwise (two electron transfer steps) or in one single step involving the transfer of two electrons accompanied by a synchronous proton transfer step (Scheme 1). It is important to note that these processes occur over a >500 mV potential range corresponding to a change in free energy of about 10 kcal/mol per single electron transfer [4,5]. Still, the working mechanism of many flavoenzymes has not yet been fully elucidated.

Both the redox properties and activity of the flavin moiety in different enzymes are largely affected by the microenvironment surrounding the isoalloxazine system [6,7], and the role of hydrogen bonding [8], aromatic π–π stacking [9], steric effects [10,11], charge transfer interactions [12] and complexation with metal ions [13] in determining such variations has been investigated. It is well documented that, in certain flavoenzymes, the photoinduced electron transfer processes take place between the isoalloxazine portion and neighbouring amino acid residues such as tryptophane and histidine [10,14]. In such process, the aforementioned interactions play an important role that is worth investigating. Bearing this in mind, the purpose of the work described here was to study in simple models the role of electronic interactions as revealed by the electrochemical and photophysical properties of isoalloxazines. We propose the use of closed cyclophane-like structures in order to somehow control the distance and orienta-

* Corresponding author. Tel.: +39 051 2099460; fax: +39 051 2099456.
E-mail addresses: gianluca.accorsi@isof.cnr.it (G. Accorsi), afarran@bec.uned.es (A. Farrán), francesco.paolucci@unibo.it (F. Paolucci), epinilla@quim.ucm.es (E. Pinilla), mrtorres@quim.ucm.es (M.R. Torres).
[1] Tel.: +39 051 6399816; fax: +39 051 6399844.
[2] Tel.: +34913988961; fax: +34913988372.
[3] Tel.: +39 051 2099460; fax: +39 051 2099456.
[4] Tel.: +34 913944285; fax: +34 913944352.

1010-6030/$ – see front matter © 2009 Elsevier B.V. All rights reserved.
doi:10.1016/j.jphotochem.2009.01.012

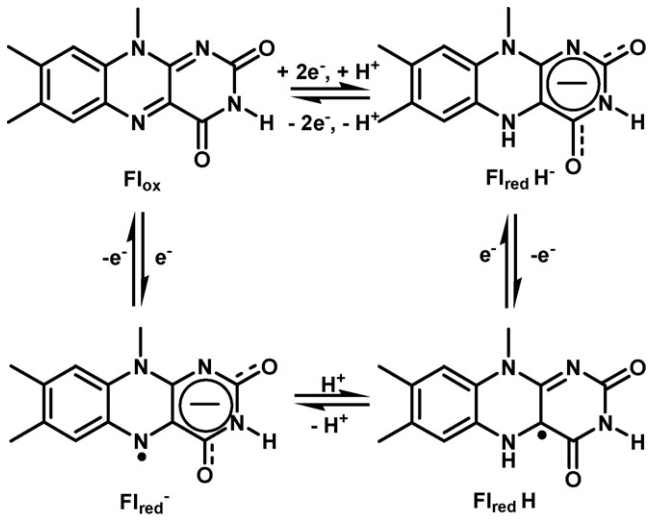

Scheme 1. Redox processes of flavins.

tion of the two chromophores involved. Reports on cyclophanes containing isoalloxazines [15–17] and dyads of isoalloxazines bridged with naphthalene and anthracene are available [18]. However, to our knowledge, no thorough study has been published yet on the intercomponent interactions occurring in such systems.

Excited state quenching of flavins like lumiflavin (7,8-dimethyl-10-methylisoalloxazine) or lumichrome (7,8-dimethylalloxazine) can take place when the counterpart is an aromatic or aliphatic amine [19]. For instance, the reduction for the lumiflavin (fluorescence quantum yield $\Phi_S = 0.16$, lifetime $\tau_S = 7.7$ ns) is observed at $E^{red}_{1/2}$ −0.7 V vs. SCE and the singlet level S lies at 2.54 eV [20]. On these basis, the low oxidation potential, $E^{ox}_{1/2}$ <+1.1 V vs. SCE for most amines [20], is expected to allow an effective photoinduced electron transfer process, resulting in quenching of the lumiflavin fluorescence [19]. Remarkably, the energy content of the triplet level of lumiflavin [3,21,22] might also be high enough to drive the quenching by electron transfer in the presence of amines featuring low oxidation potentials. Furthermore, aromatic compounds like the dimethoxybenzenes, with $E^{ox}_{1/2}$ in the range +1.3 to +1.5 V vs. SCE, can act as effective quenchers of the fluorescent excited states of flavins [19]. When studying photoinduced electron transfer for couples constituted by flavins and aromatic compounds one should mind about the possible occurrence of competing energy transfer steps [23,24]. In fact, in the presence of suitable compounds, decay of the singlet level of the flavin unit is expected to occur via a number of competing steps. These are (i) intramolecular intersystem crossing (ISC), to populate the flavin triplet level, (ii) intercomponent electron transfer, provided energy requirements are met, as seen above, and (iii) intercomponent energy transfer, provided an energy level both of singlet (S) or triplet (T) nature lying lower than E_S (i.e., of the flavin unit) is present on the other component (see below).

In order to precisely investigate the electron transfer quenching of the S level of a flavin derivative, **FL6**, we have designed and prepared bichromophores wherein the aromatic counterparts are 2-methoxynaphthalene, **mona**, and 2,7-dimetoxynaphhalene, **dmona**, Scheme 2, also collectively denoted as oxynaphthalenes, **ona**. For the latter compounds, the fluorescent level E_S is >3.8 eV and the phosphorescent level E_T is ∼2.6 eV [6,7]. Thus, given that the energy content of S_{FL6} is ca. 2.6 eV (see below), the $S_{FL6} \rightarrow S_{ona}$ energy transfer step is energetically unfavoured while $S_{FL6} \rightarrow T_{ona}$ is barely isoergonic. Therefore, the only exothermic process that can effectively quench the S_{FL6} level is photoinduced electron transfer. Bearing in mind diffusional studies performed before [19], we have monitored intramolecular photoinduced electron transfer processes in both open and closed bichromophores, **OFn** and **MFn**, respectively with $(CH_2)_n$ spacers linking the two interacting units ($n = 4$ or 6, Scheme 2). According to molecular models, the center-to-center interchromophore separation was estimated in the range of 5–9 Å for the two open forms **OF4** and **OF6** (with a wide conformer distribution) and the two closed macrocyclic forms **MF4** and **MF6** (with a narrower conformer distribution).

2. Experimental

2.1. Equipment

Melting points were determined using a ThermoGalen hot stage microscope. Unless otherwise stated, column chromatography was performed on silica gel (Merck 60, 70–230 mesh). The R_f values were measured on aluminium coated silica gel 60 F254 TLC plates (Merck, 0.2 mm) with the indicated eluent. Mass spectra were performed in a FAB Waters VG Autospec (UAM-SIDI) using m-nitrobenzylic alcohol as matrix. Elemental analysis for carbon, hydrogen and nitrogen were carried out by the CAI-UCM Microanalytical Service on a PerkinElmer 240 Analyzer. Spectra were recorded in a Bruker DRX 400 (9.4T, 400.13 MHz for ^{1}H and 100.62 MHz for ^{13}C NMR) spectrometer. Chemical shifts (δ in ppm) are given from internal $CHCl_3$ (7.26 ppm) for ^{1}H NMR, $^{13}CDCl_3$ (77 ppm) for ^{13}C NMR Coupling constants (J in Hz) are accurate to a ±0.2 Hz for ^{1}H.

2.2. Syntheses of flavin derivatives

2.2.1. 3,10-dihexyl-8-(hexyloxy)benzo[g]pteridine-2,4(3H,10H)-dione (*FL6*)

1 g (3.2 mmol) of 10-hexyl-8-hydroxyisoalloxazine (**FL**) was suspended in 20 mL of dry dimethylformamide, then 10 eq (32 mmol, 5.12 g) of 1-bromohexane and 10 eq (32 mmol, 4.42 g) of potassium carbonate were added to the solution. The mixture was heated under Ar atmosphere at 90 °C for 24 h. The reaction mixture was filtered through a celite pad and DMF was removed under reduced pressure. The remaining solid was purified by column chromatography using as eluent, at first hexane to eliminate the excess 1-bromohexane and then a 1:100 methanol dichloromethane mixture. A yellow solid **FL6** (1.4 g) was obtained with a 90% yield m.p. = 136 °C Anal. Cald for $C_{29}H_{46}N_4O_3$: C 69.68; H. 8.67; N 11.61 Found: C 69.12; H.8.66; N 11.48.

^{1}H NMR ($CDCl_3$) δ ppm 8.19 (d, 1H, H-6, $J = 9.1$ Hz), 7.18 (dd, 1H, H-7, $J = 9.1$ Hz, $J = 2.4$ Hz), 6.89 (d, 1H, H-9, $J = 2.4$ Hz), 4.62 (m, 2H, N-10-C*H*$_2$(CH$_2$)$_4$CH$_3$), 4.16 (t, 2H, C-8-OC*H*$_2$(CH$_2$)$_4$CH$_2$CH$_3$, $J = 6.5$ Hz), 4.08 (t, 2H, N-3-C*H*$_2$(CH$_2$)$_4$ CH$_2$CH$_3$, $J = 6.5$ Hz) 1.87 (m, 4H, (CH$_2$)), 1.70 (m (b), 2H, (CH$_2$)), 1.52 (m, 4H, (CH$_2$)), 1.33 (m, 14H, (CH$_2$)) 0.91 (t, 9H, C*H*$_3$, $J = 6.8$ Hz).

^{13}C NMR ($CDCl_3$) δ ppm ($CDCl_3$) 165.2, 155.8, 150.1, 135.3, 133.5, 131.4, 116.2, 98.3, 69.4, 45.5, 41.7, 31.6, 31.4, 31.4, 31.4, 28.9, 27.8, 26.6, 26.6, 26.5, 25.6, 22.5, 22.5, 14.1, 13.9.

2.2.2. 2-(hexyloxy)naphtalene (*mona*)

1 g (6.94 mmol) of 2-naphtol was dissolved in 20 mL of dry acetonitrile and 1.2 eq (8.33 mmol, 1.375 g) of 1-bromohexane and 2 eq (13.88 mmol, 4.5 g) of cesium carbonate were added to the solution that was heated overnight at 80 °C. The reaction mixture was filtered a through celite pad and the solvent removed under reduced pressure. The residue was purified by column chromatography (hexane:CH_2Cl_2, 3:1). **mona** was obtained as a white solid (1.42 g, 90% yield) that was recrystallized from methanol to afford

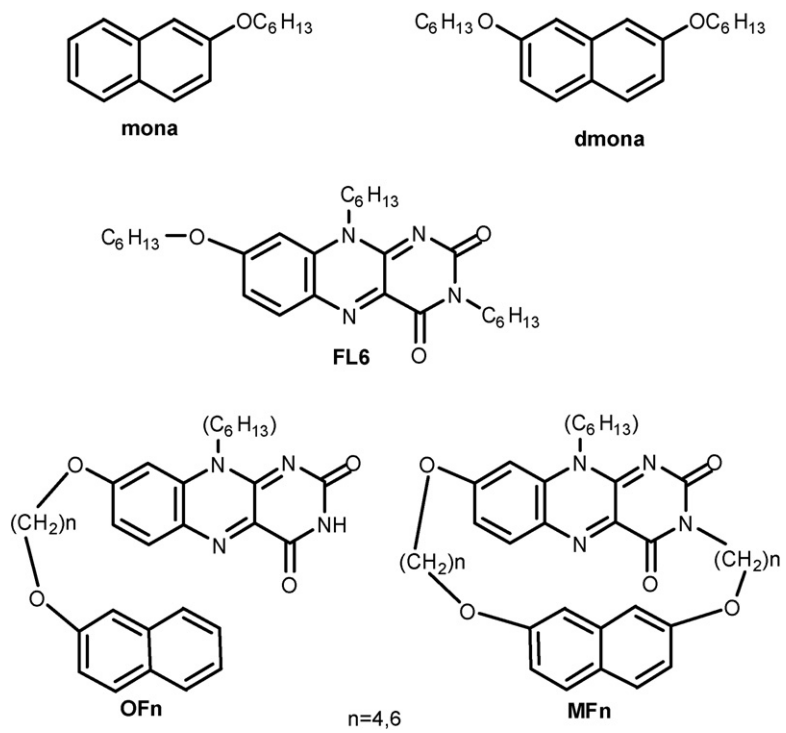

Scheme 2. Molecular structures of compounds under study.

mona as a white solid. m.p. = 32 °C Anal. Cald for $C_{16}H_{20}O$: C 84.16; H. 8.83 Found: C 83.9; H. 8.78.

^{1}H NMR ($CDCl_3$) δ ppm 7.76 (3H, m, H-19, H-20, H-21), 7.45 (1H, t, H-23, J = 7.0 Hz), 7.34 (1H, ddd, H-22, J = 8.1, J = 7.0, J = 1.4 Hz), 7.17 (2H, m, H-18, H-24), 4.09 (2H, t, OCH_2(CH_2)$_4$$CH_3$, J = 6.6 Hz), 1.87 (2H, m, CH_2)), 1.52 (2H, m, (CH_2)), 1.39 (4H, m, (CH_2)), 0.95 (3H, t, CH_3, J = 7.0 Hz).

^{13}C NMR ($CDCl_3$) δ ppm 157.1, 134.5, 129.3, 128.8, 127.6, 127.5, 126.6, 123.3, 118.9, 105.6, 67.9, 31.6, 29.3, 25.8, 22.5, 14.1.

*2.2.3. 2,7-bis(hexyloxy)naphtalene (**dmona**)*

1 g (6.94 mmol) of 2-naphtol was dissolved in 20 mL of dry acetonitrile then 5 eq (34.7 mmol, 5.75 g) of 1-bromohexane and 5 eq (34.7 mmol, 11.3 g) of cesium carbonate were added to the solution. The reaction mixture was heated overnight at 80 °C. The reaction mixture was filtered through a celite pad and the solvent removed under reduced pressure. The residue was purified by column chromatography (hexane:CH_2Cl_2, 5:1). **dmona** was obtained as a yellowish solid (1.84 g, 90% yield) that was recrystallized from methanol to afford **dmona** as a white solid. m.p. = 42 °C Anal. Cald for $C_{22}H_{32}O_2$: C 80.44; H. 9.82 Found: C 80.12; H.9.65.

^{1}H NMR ($CDCl_3$) δ ppm 7.64 (2H, d, H-19, H-20, J = 7.6 Hz), 7.03 (2H, d, H-23, H-24, J = 2.4 Hz), 6.98 (2H, dd, H-18, H-21, J = 8.8 Hz, J = 2.4 Hz), 4.06 (4H, t, O-CH_2(CH_2)CH_3, J = 6.6 Hz), 1.84 (4H, m, (CH_2)), 1.49 (4H, m, (CH_2)), 1.37 (8H, m, (CH_2)), 0.93 (6H, t, CH_3, J = 7.0 Hz).

^{13}C NMR ($CDCl_3$) δ ppm 157.7, 136.0, 129.0, 124.1, 116.0, 106.0, 99.9, 68.0, 31.6, 29.2, 25.8, 22.6, 14.0.

*2.2.4. 10-butyl-3-methyl-8-(6-(naphthalen-2-yloxy)butyloxy)benzo[g]pteridine-2,4(3H,10H)-dione (**OF4**)*

0.5 g (1.52 mmol) of 10-hexyl-8-hydroxy-3-methyl isoalloxazine and 0.219 g (1.52 mmol) of 2-naphtol were dissolved in 50 mL of dimethylformamide, then 5 eq (7.6 mmol, 1.05 g) of potassium carbonate and 5 eq (7.6 mmol, 1.04 g) of 1,4-dibromobutane added to the solution. The reaction mixture was heated overnight at 80 °C. The reaction mixture was then filtered through a celite pad and the solvent evaporated under reduced pressure. The residue was purified by column chromatography (9:1 CH_2Cl_2:EtOAc) to afford 30% (290 mg) of **OF4** (as well as the two other statistical products, di-isoalloxazine and di-naphtol) m.p. = 122 °C FAB-MS m/z = 527.56 [M + H$^+$] Anal. Cald for $C_{31}H_{34}N_4O_4$: C 70.70; H. 6.51; N 10.64; Found: C 70.40; H. 6.56; N 10.38.

^{1}H NMR ($CDCl_3$) δ ppm 8.21 (1H, d, H-6, J = 9.1 Hz), 7.73 (3H, m, H-19, H-20, H-21, J = 8.9 Hz), 7.42 (1H, t, H-23, J = 7.5 Hz), 7.34 (1H, t, H-22, J = 6.8 Hz), 7.19 (1H, H-7, d, J = 9.1 Hz), 7.10 (2H, m, H-24, H-18), 6.86 (1H, d, H-9, J = 2.4 Hz), 4.58 (2H, s, N-10-CH_2(CH_2)$_2$$CH_3$), 4.30 (2H, t, C-8-O-$CH_2$, J = 6.5 Hz), 4.20 (2H, t, C-17-O-CH_2, J = 6.6 Hz), 3.52 (3H, s, N-3-CH_3), 2.12 (2H, m, (CH_2)), 1.97 (4H, m), 1.34 (6H, m, (CH_2)), 0.90 (3H, t, N-10-(CH_2)$_5$-CH_3, J = 7.0 Hz).

^{13}C NMR ($CDCl_3$) 165.1, 160.3, 156.7, 156.2, 148.9, 135.2, 134.8, 134.4, 133.3, 131.7, 129.5, 128.9, 127.7, 126.6, 126.4, 123.7, 118.6, 115.8, 106.6, 98.3, 68.9, 67.1, 44.6, 31.5, 28.7, 26.6, 26.5, 25.9, 25.8, 22.5, 13.9.

*2.2.5. 10-hexyl-3-methyl-8-(6-(naphthalen-2-yloxy)hexyloxy)benzo[g]pteridine-2,4(3H,10H)-dione (**OF6**)*

0.5 g (1.52 mmol) of 10-hexyl-8-hydroxy-3-methyl isoalloxazine and 0.219 g of 2-naphtol (1.52 mmol) were dissolved in 50 mL of dimethylformamide, then 5 eq (7.6 mmol, 2.46 g) of cesium carbonate and 5 (7.6 mmol, 1.25 g) eq of 1,6-dibromohexane added to the solution. The reaction mixture was heated overnight at 80 °C. The reaction mixture was then filtered through a celite pad and the solvent evaporated under reduced pressure. The residue was purified by column chromatography (9:1 CH_2Cl_2:EtOAc) to afford 30% (250 mg) of **OF6** (as well as the two other statistical products, di-isoalloxazine and di-naphtol) m.p. = 145 °C FAB-MS m/z = 555.29 [M + H$^+$] Anal. Cald for $C_{33}H_{38}N_4O_4$: C 71.46; H, 6.91; N, 10.10 Found: C 70.93; H, 6.93; N, 10.0.

^{1}H NMR ($CDCl_3$) δ ppm 8.20 (1H, d, H-6, J = 9.1 Hz), 7.71 (3H, m, H-19, H-20, H-21, J = 8.9 Hz), 7.68 (2H, H-19, H-20), 7.41 (1H, H-23, t, J = 8.0 Hz), 7.32 (1H, t, H-22, J = 8.0 Hz), 7.19 (1H, d, H-7, J = 9.1 Hz),

7.11 (1H, m, H-18, H-24), 6.87 (1H, d, H-9, J = 2.4 Hz), 4.61 (2H, s, N-10-CH_2), 4.13 (6H, m, C-17-OCH_2, C-8-OCH_2), 3.52 (3H, s, N-3-CH_3), 1.88 (4H, m, (CH_2)), 1.54 (m, 4H, (CH_2)), 1.50 (m, 4H, (CH_2)), 1.36 (m, 4H, (CH_2)), 0.91 (3H, t, N-10-$(CH_2)_5$-CH_3, J = 7.0 Hz).

^{13}C NMR ($CDCl_3$) δ ppm 165.5, 160.1, 156.9, 156.3, 155.4, 149.0, 135.2, 135.1, 133.1, 131.7, 129.3, 128.9, 127.6, 126.6, 126.4, 118.8, 116.3, 106.7, 98.4, 69.4, 67.7, 44.9, 31.7, 29.3, 29.1, 28.9, 28.8, 26.8, 26.7, 26.0, 25.8, 25.7, 25.6, 22.7, 14.2.

2.2.6. 1-^{10}hexyl-6,8,13-trioxa-1^2 H-1(3,8)benzo[g]pteridina-7(2,7)-naphtalenacyclotridecaphane-1^2,1^4(1 ^{10}H)-dione (***MF4***)

0.8 g (2.54 mmol) of 10-hexyl-8-hydroxyisoalloxazine (**FL**), 1.01 g (2.54 mmol) of 2,7-bis(4-bromobutyloxy)naphthalene was dissolved in 300 mL of dry dimethylformamide, then, 3.52 g (25.4 mmol) of potassium carbonate was added. The reaction mixture was stirred at 80 °C for 72 h, then filtered through a celite pad and the solvent removed by vacuum distillation. The residue was purified using column chromatography using as eluent CH_2Cl_2:ethylacetate, 9:1. 150 mg (10% yield) of **MF4** were obtained that were further purified by recrystallization in acetonitrile. m.p. = 209 °C FAB-MS m/z = 583.1 [M + H$^+$] Anal. Cald for $C_{34}H_{38}N_4O_5$ C. 70.08; H. 6.57; N. 9.62 Found: C 69.29; H. 6.58; N. 9.06.

^{1}H NMR ($CDCl_3$) 8.19 (1H, d, H-6, J = 9.1 Hz), 7.58 (2H, d, H-19, J = 8.9 Hz, J = 5.5 Hz), 7.21 (dd, 1H, H-7, J = 9.1 Hz, J = 2.4 Hz), 6.95 (1H, dd, H-21, J = 8.9 Hz, J = 2.4 Hz), 6.90 (1H, dd, H-18, J = 8.8 Hz, J = 2.4 Hz), 6.22 (1H, d, H-9, J = 2.4 Hz), 5.91 (1H, H-24, d, J = 2.4 Hz), 5.70 (1H, H-23, d, J = 2.4 Hz), 4.64 (1H, m, a), 4.52 (1H, t, O-22-CH_2 d, J = 9.0 Hz), 4.39 (1H, t, O-8-CH_2 a′, J = 9.0 Hz), 4.28 (1H, m, N-3-CH_2, e), 4.13 (4H, m, d′, e′, e, i), 3.82 (2H, m, O-17-CH_2, h, h′), 3.15 (1H, s (b), N-10-CH_2, i′), 2.41 (2H, m, (CH_2)), 2.06 (6H, m, (CH_2)), 1.20 (8H, m), 0.86 (3H, t, N-10-$CH_2(CH_2)_4CH_3$, J = 7.0 Hz).

^{13}C NMR ($CDCl_3$) δ ($CDCl_3$) 164.1, 161.1, 157.5, 156.1, 155.6, 148.4, 135.1, 134.5, 133.3, 131.2, 129.5, 128.8, 123.8, 116.2, 114.1, 110.4, 109.1, 104.4, 100.7, 69.1, 66.6, 43.7, 41.5, 31.1, 29.7, 27.4, 26.2, 26.1, 25.9, 23.8, 22.4, 22.0, 13.9.

2.2.7. 1-^{10} hexyl-8,10,17-trioxa-1^2 H-1(3,8)benzo[g]pteridina-7(2,7)-naphtalenacycloheptadecaphane-1^2,1^4(1 ^{10}H)-dione (***MF6***)

0.8 g (2.54 mmol) of 10-hexyl-8-hydroxyisoalloxazine, 1.235 g (2.54 mmol) of 2,7-bis(6-bromohexyloxy)naphthalene were dissolved in 300 mL of dry DMF, then, 10 eq (25.4 mmol, 3.52 g) of potassium carbonate. The reaction mixture was stirred at 80 °C for 72 h, then filtered through a celite pad and the solvent removed by vacuum distillation. The residue was purified by column chromatography (silica gel) using as eluent CH_2Cl_2:ethylacetate (90:10) and 160 mg (10% yield) of **MF6** were obtained that were further purified by recrystallization in acetonitrile m.p. = 222 °C FAB-MS m/z = 639.80 [M + H$^+$] Anal. Cald for $C_{38}H_{46}N_4O_5$ C. 71.45; H. 7.26; N. 8.77 Found: C. 70.78; H. 7.16; N. 8.58.

^{1}H NMR ($CDCl_3$) δ ppm 8.11 (1H, d, H-6, J = 9.1 Hz), 7.57 (dd, 2H, H-19-H-20, J = 5.60, 8.9 Hz), 7.14 (d, H, H-7, J = 9.1, J = 2.4 Hz), 6.92 (d, 2H, H-18-H-21, J = 8.9 Hz, J = 2.4 Hz), 6.74 (d, 1H, H-9, J = 2.4 Hz), 6.57 (d, 1H, H-24, J = 2.4 Hz), 6.49 (d, 1H, H-23, J = 2.4 Hz), 4.30 (m, 6H, N-3-$CH_2(CH_2)_4CH_2$-O-17 N-10-$CH_2(CH_2)_4$, C-8-CH_2-$(CH_2)_4$-CH_3), 3.91 (t, 2H, C-22-O-CH_2, J = 6.0 Hz), 3.76 (t, 2H, O-17-CH_2, J = 6.6 Hz), 1.88 (m, 4H, (CH_2)), 1.78 (m, 4H, (CH_2)), 1.57 (m, 6H, (CH_2)), 1.42 (m, 4H, (CH_2)), 1.27 (m, 4H, (CH_2)), 1.19 (m, 6H, (CH_2)), 0.82 (t, 3H, CH_3, J = 7.0 Hz).

^{13}C NMR ($CDCl_3$) δ ppm 165.0, 160.4, 157.8, 157.1, 156.0, 148.9, 135.6, 135.1, 134.7, 133.2, 131.6, 129.1, 129.0, 124.1, 116.9, 115.3, 114.5, 107.1, 105.4, 99.1, 68.2, 67.6, 66.8, 44.3, 41.2, 31.1, 28.4, 28.1, 28.0, 27.0, 26.4, 26.3, 26.6, 25.6, 25.2, 24.7, 24.5, 24.4, 22.5, 13.9.

2.3. Spectroscopic measurements

Absorption spectra were recorded with a PerkinElmer λ9 spectrophotometer in CH_2Cl_2 solvent. For luminescence experiments in the same solvent, the samples were placed in fluorimetric cm^{-1} path cuvettes. Uncorrected emission spectra were obtained with an Edinburgh FLS920 spectrometer equipped with a peltier-cooled Hamamatsu R928 photomultiplayer tube (185–850 nm). An Edinburgh Xe900 450 W Xenon arc lamp was used as exciting light source. Corrected spectra were obtained via a calibration curve supplied with the instrument. Luminescence quantum yields (ϕ_{em}) in solution obtained from spectra on a wavelength scale (nm) were measured according to the approach described by Demas and Crosby [28] using air-equilibrated [Ru(bpy)$_3$Cl$_2$ in water solution ϕ_{em} = 0.028] [29] as standard.

Emission lifetimes were determined with the single photon counting technique by means of the same Edinburgh FLS920 spectrometer using a laser diode as excitation source (1 MHz, λ_{exc} = 407 nm, 200 ps time resolution after deconvolution) and the above-mentioned PMTs as detector. To record the 77 K luminescence spectra, the samples were put in glass tubes (2 mm diameter) and inserted in a special quartz dewar, filled up with liquid nitrogen. Experimental uncertainties are estimated to be ±8% for lifetime determinations, ±20% for emission quantum yields, ±2 and ±5 nm for absorption and emission peaks respectively.

2.4. Electrochemical measurements

Tetrabutylammonium hexafluorophosphate (TBAH) was used as received as supporting electrolyte, and was electrochemical or analytical grade from Fluka. Tetrahydrofuran (THF) was purified and dried as previously reported [30], stored in a specially designed Schlenk flask and protected from light.

Electrochemical experiments were carried out in an airtight single-compartment cell described elsewhere [31], using platinum disc (with diameter of 125 μm) as working, a platinum spiral as counter electrodes and a silver spiral as a quasi-reference electrode. The drift of the quasi-reference electrode was negligible during the time required for an experiment. All the $E_{1/2}$ potentials have been directly obtained from cyclic voltammetric curves as averages of the cathodic and anodic peak potentials and by digital simulation for those processes, which are not Nernstian, or for processes closely spaced in multielectron voltammetric peaks. The $E_{1/2}$ values, referenced to the aqueous saturated calomel electrode (SCE), have been determined by adding ferrocene at the end of each experiment as an internal standard and measuring them with respect to the ferrocinium/ferrocene couple standard potential. The cell containing the supporting electrolyte and the electroactive compound was dried under vacuum at 100–110 °C for at least 60 h before each experiment. The pressure measured in the electrochemical cell prior to performing the trap-to-trap distillation of the solvent was typically 1–2 × 10^{-5} mbar. Voltammograms were recorded with an AMEL Mod. 552 potentiostat [32] or a custom made fast potentiostat controlled by an AMEL Mod. 568 programmable function generator. The potentiostat was interfaced to a Nicolet Mod. 3091 digital oscilloscope and the data transferred to a personal computer by the program Antigona [33]. Minimization of the uncompensated resistance effect in the voltammetric measurements was achieved by the positive-feedback circuit of the potentiostat. Digital simulations of the cyclic voltammetric curves were carried out either by Antigona or DigiSim 3.0 (Bioanalytical Systems Inc.).

2.5. X-ray data collection and structure refinement

Suitable needle crystals of **MF4** for X-ray diffraction experiments were obtained by crystallization from *N*,*N*-

dimethylformamide/water. Many attempts were made to obtain crystals of **MF6** of good quality. However, only crystals polysynthetically twined could be obtained. In spite of this, we considered of much interest to analyze them in order to experimentally validate the center-to-center interchromophores (naphthalene and isoalloxazine) distances predicted by Molecular Mechanics calculations. Data collection for both compounds was carried out at room temperature on a Bruker Smart CCD diffractometer using graphite-monochromated Mo Kα radiation (λ = 0.71073 Å) operating at 50 kV and 30 mA. In both cases, data were collected over a hemisphere of the reciprocal space by combination of three exposure sets. Each exposure of 30 s covered 0.3 in ω for **MF4** and for **MF6** different exposure times were used in different data collection, and the best results, although still not ideal, correspond to 10 s. The cell parameters were determined and refined by a least-squares fit of all reflections. The first 100 frames were recollected at the end of the data collection to monitor crystal decay, and no appreciable decay was observed.

A summary of the fundamental crystal and refinement data is given in Table 1. The structures were solved by direct methods and conventional Fourier techniques, and refined by full-matrix least squares procedures on F^2 for **MF4** and full cycle-matrix least squares procedures on F^2 for **MF6** (SHELXL-97) [34]. Anisotropic parameters were used in the last cycle of refinement for all non-H atoms with exceptions. For **MF6**, the carbon atoms chains were refined using geometrical restrains and variable common carbon–carbon distances in three anisotropical cycles, and in subsequent cycles their thermal parameters were kept constant. For **MF4** after the last cycles of refinement, some diffuse electronic density was located at the Fourier difference and several models were tried to solve this disorder of the solvent, but could not be properly modeled. For this fact, the SQUEEZE program, a part of the PLATON [35] package of crystallographic software, was used to calculate the solvent disorder area and remove its contribution to the overall intensity data. An improvement was observed in all refinement parameters and residuals when this procedure was applied. The number of electrons in the solvent region corresponding to a dimethylformamide molecule per **MF4** molecule in the crystal. The hydrogen atoms were included in calculated positions and refined riding on the respective carbon atoms. These features led to *R* values depicted in Table 1.

Table 1
Crystal data and structure refinement for compounds **MF4** and **MF6**.

Crystal data	MF4	MF6
Identification code	CCDC-689193	CCDC-689194
Empirical formula	$C_{34}H_{38}N_4O_5$	$C_{38}H_{46}N_4O_5$
Formula weight	582.68	638.79
Wavelength (Å)	0.71073	0.71073
Crystal system	Orthorhombic	Monoclinic
Space group	P2(1)2(1)2(1)	P2(1)/n
Unit cell dimensions		
a (Å)	8.3708(9)	14.4688(8)
b (Å)	19.683(2)	23.950(1)
c (Å)	20.005(2)	20.059(1)
β (°)	–	99.704(2)
Volume (Å^3)	3296.1(6)	6851.3(6)
Z	4	8
Density (calculated) (Mg/m^3)	1.174	1.239
Absorption coefficient	0.080 (mm^{-1})	0.083 (mm^{-1})
F(0 0 0)	1240	2736
Theta range (°)	1.45–25.0	1.34–25.57
Index ranges	$-9 <= h <= 9$ $-22 <= k <= 21$ $-23 <= l <= 23$	$-17 <= h <= 17$ $-27 <= k <= 27$ $-22 <= l <= 22$
Reflections collected	23737	49473
Independent reflections	5488[*R*(int) = 0.1865]	11630[*R*(int) = 0.1920]
Data/restraints/parameters	5488/0/390	11630/3 0/586
$R^a[I > 2\sigma(I)]$	0.0692 (1360 obs. reflect.)	0.1152 (2026 obs. reflect.)
$Rw_F{}^b$ (all data)	0.1747	0.4675

[a] $\sum||F_o| - |F_c||/\sum|F_o|$.

[b] $\left\{\sum[w(F_o^2 - F_c^2)^2]/\sum[w(F_o^2)^2]\right\}^{1/2}$.

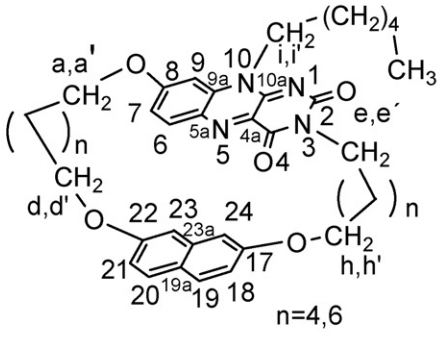

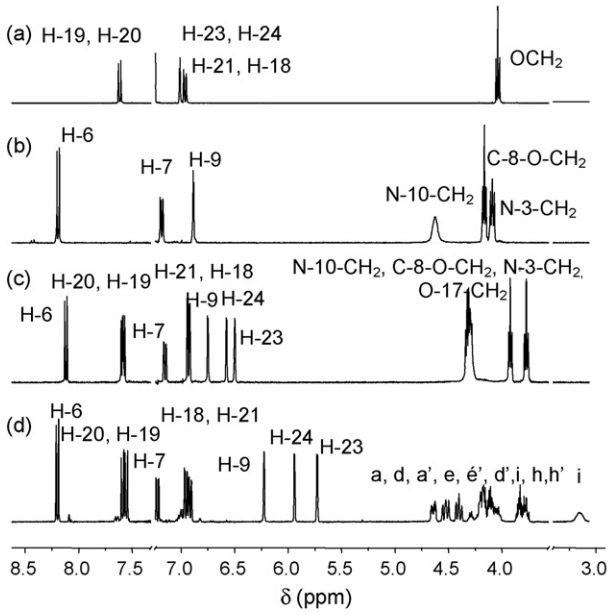

Fig. 1. ^{1}H NMR spectra in $CDCl_3$ of (a) **dmona**, (b) **FL6**, (c) **MF6** and (d) **MF4**.

2.6. MM calculations

MacroModel v. 8.1, with the GB/SA model for chloroform was used in order to perform the molecular simulations of **OFn** and **MFn** in all cases. All calculations were achieved with Monte Carlo (MC) conformational analyses. Previously to MC all molecules were energy-minimized. Minimization is carried out using Polak-Ribiere conjugate gradient optimiser. In a typical MC run a MCMM is performed with, at least, 1000 steps for each degree of freedom, this leads to a MC run between 10,000 and 20,000 steps. The force field used in these calculations was AMBER as implemented in the version of the programme.

3. Results and discussion

3.1. Syntheses

Cyclophanes **MFn** and open structures **OFn** used in this work were prepared from previously synthesized 10-hexyl-

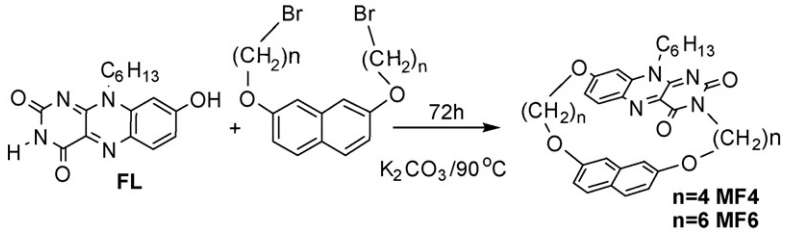

Scheme 3. Synthetic route leading to **MF4** and **MF6**.

8-hydroxyisoalloxazine [25] using the procedure reported by Diederich et al. [15–18] and Yoneda et al. [26] The model naphthalenes **mona** and **dmona** were prepared by a standard alkylation procedure from commercially available 1-naphtol (for **mona**) and 2,7-dihydroxynaphtalene (for **dmona**). **FL6** was prepared by simple alkylation with 6-bromohexane from 10-hexyl-8-hydroxyisoalloxazine. **OFn** were prepared by reaction of 10-hexyl-8-hydroxy-3-methylisoalloxazine and 1-naphtol in the presence of 1,4-dibromobutane (**OF4**) or 1,6-dibromohexane using cesium carbonate as base obtaining a statistical mixture being **OFn** isolated from the mixture by column chromatography.

The synthetic route depicted in Scheme 3 was the one used to obtain **MF4** and **MF6**.

All compounds were structurally characterized by NMR spectroscopy (Fig. 1). As predicted by the molecular modelling experiments, the two chromophores, the flavin and the naphtalene ring in the macrocyclic structures have a preferred conformation. In **MF4** the distances between them are smaller and the anisotropic ring currents due to π–π stacking cause shielding for protons H-9, H-23 and H-24 that are pointing towards the inner cavity of the macrocyclic structure. The same effect is observed in **MF6** but somehow less pronounced since the distances are longer and a smaller

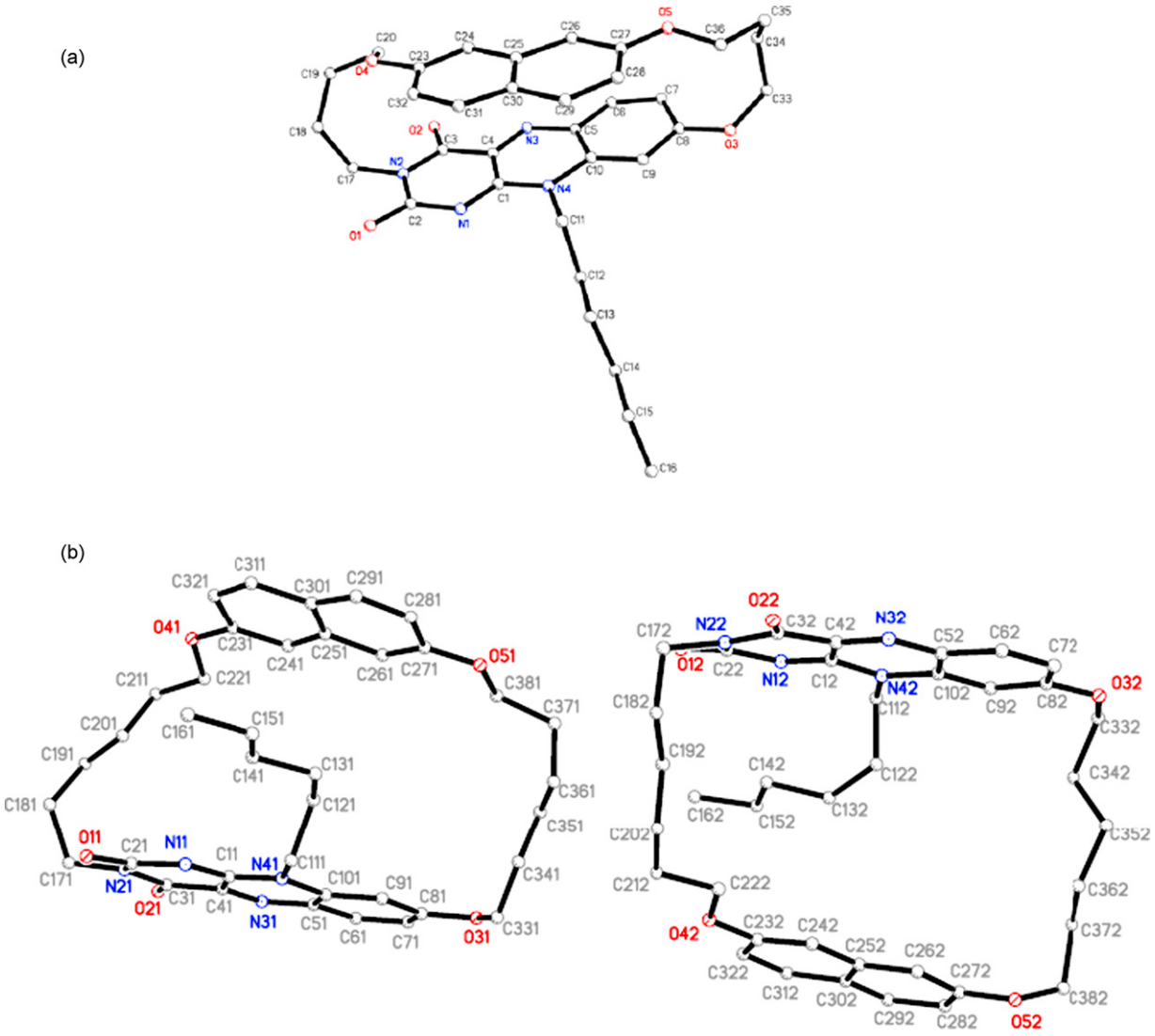

Fig. 2. (a) an **MF4** molecule in the asymmetric unit showing the X-ray atom numbering, (b) the two different conformations of **MF6** molecule in the asymmetric unit showing the X-ray atom numbering.

shift is observed (close contacts measured N-10 to C-19, in **MF4** 3.58 and 5.56 Å in **MF6**). The aliphatic protons that link the two chromophores become diasterotopic in **MF4** and assignments were based on the correlations found in NOE experiments that can be found in Supplementary material.

3.2. X-ray crystal structures

Pluto perspectives of the molecular structures of **MF4** and **MF6** with the atomic numbering are shown in Figs. 2 and 3. In the structural determination, one crystallographic independent molecule for asymmetric unit was identified in **MF4**. Differently, in **MF6** two independent conformations were found, due to a dissimilar relative disposition of the isoalloxazine and naphthalene: in conformation 1, the torsion angle between both groups is 30.61° while, in conformation 2, they are almost eclipsed. In the case of **MF4**, similar features as those found in the case of molecule 2 of **MF6** exists. The fact that **MF4** crystallizes in a conformation of type 2 (eclipsed) while **MF6** crystallizes in two conformations, one of type 2 (eclipsed) and the other of type 1 (twisted) is related to the length linking both aromatic rings. The shorter $n = 4$ would allow only for the eclipsed structure and the longer $n = 6$ for both, eclipsed and twisted, structures. Crystal packing forces determine compact conformations.

For both compounds **MF4** and **MF6**, the best least-square planes for the naphthalene and isoalloxazine moieties, that are planar within the experimental error (maximum deviation is 0.100 (6) Å for C2 of **MF4**), are stacked roughly parallel to each other. All rings show distances and angles as expected. The influence of the different length of the chains is observed in the distances between the rings of the isoalloxazine and naphthalene groups. For **MF4** average values between the centroids are 4.03 Å while for conformations 1 and 2 of **MF6** are 7.21 and 7.97 Å, respectively.

3.3. Cyclic voltammetry

The electrochemical properties of **OF4**, **OF6**, **MF4**, **MF6** and related model compounds **FL6**, **mona**, and **dmona** were investigated by cyclic voltammetry (CV) in ultra-dry THF; results are collected in Table 2.

The CV curves of **MF4** and **MF6** show cathodic peaks at negative potentials that can be attributed to the reduction of both flavin and oxynaphthalene moieties. Fig. 4a and b show the CV curves of **MF4** and **MF6**, respectively: the processes at −0.80 and −1.85 V (**MF4**) or −0.83 and −1.90 V (**MF6**) are both located into the flavin moiety while the processes at −2.74 V (for both **MF4** and **MF6**) are associated to the reduction of the **dmona** moiety.

This was confirmed by comparison with the CV curves of the two model compounds shown in Fig. 4d.

Interestingly, the observed shift of the corresponding reduction peaks with respect to the models is consistent with the presence of small interactions between the two moieties in both macrocycles. Such a shift was not observed in the case of open forms **OF4** and **OF6** (see, e.g., Fig. 4c). However, a quantitative evaluation of the inter-moiety interaction was made difficult by the partial irreversibility of the voltammetric pattern at the level of the flavin-centered second reduction that makes the peak position dependent on the scan rate. Such an irreversible behaviour is manifested by the presence of the anodic peak at −0.50 V in the reverse scan for both macrocycles and for the model species **FL6**, indicating a relatively fast

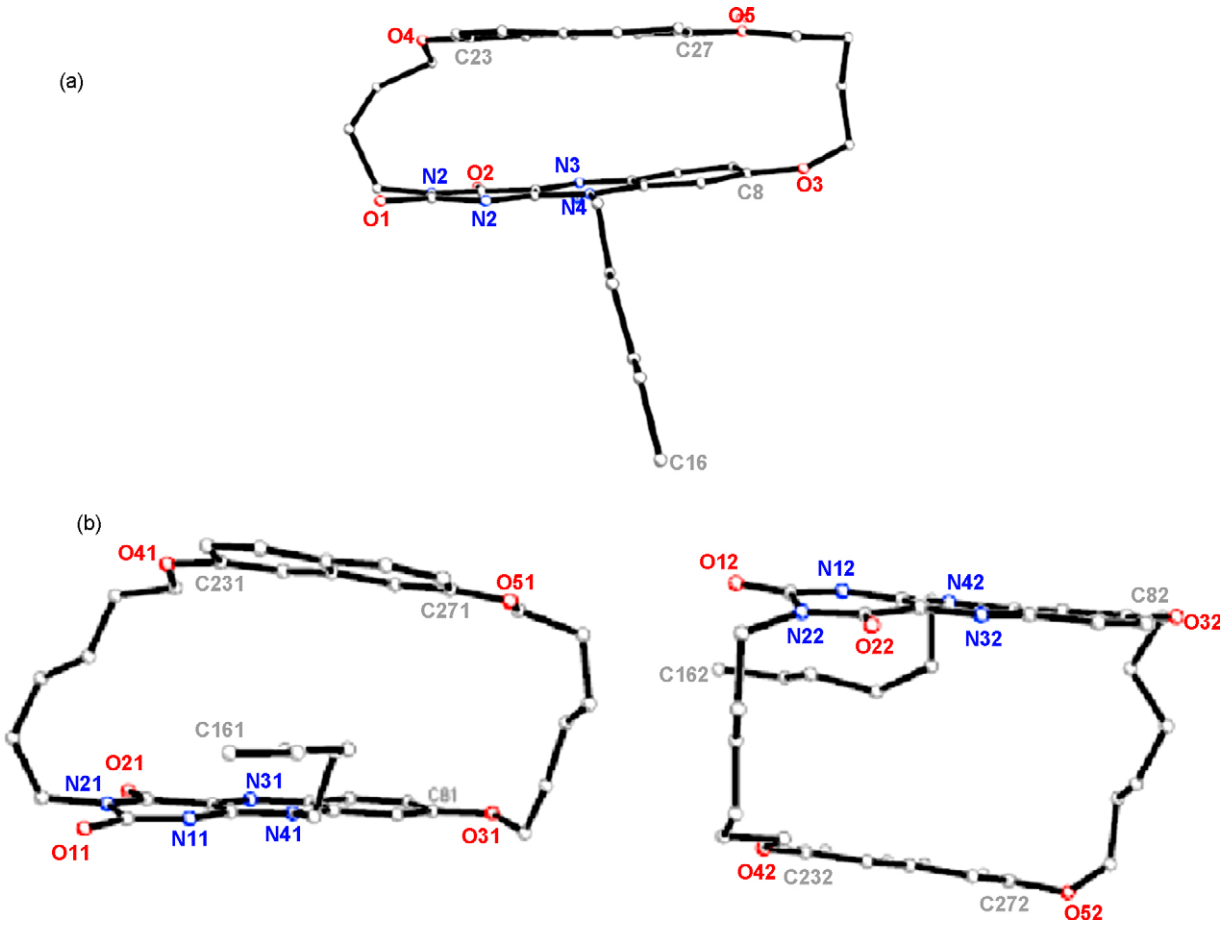

Fig. 3. Another view of (a) **MF4** and (b) **MF6**, showing the parallel disposition of the aromatic rings.

Table 2
Electrochemical data for the bichromophores and related model compounds: 1 mM in 70 mM TBAH THF (reductions) or CH_2Cl_2 (oxidations) solutions; scan rate: 1 V/s, T = 298 K, working electrode: Pt disc (125 μm diameter).

	$E_{1/2}/V$ (vs. SCE)			
MF4	+1.44	−0.80	−1.85[a]	−2.74
MF6	+1.42	−0.83	−1.90[a]	−2.74
OF4	+1.44	−0.85	−1.84	−2.62
OF6	+1.44	−0.85	−1.84	−2.62
dmona	+1.40	–	–	−2.74
mona	+1.44	–	–	−2.62
FL6	–	−0.85	−1.84[a]	–

[a] Calculated by simulation of the experimental CV curves according to the mechanism in Scheme 1 and using the kinetic parameters given in the text. Other relevant simulation parameters: $k^\circ_h = 0.1\ cm\ s^{-1}$ (first reduction of flavins), $k^\circ_h = 3 \times 10^{-3}\ cm\ s^{-1}$ (second reduction of flavins), $D = 10^{-5}\ cm^2\ s^{-1}$.

follow-up reaction coupled to the second reduction of the **FL6** moiety. In view of the known strong basicity of flavin dianion [23] the above follow-up reaction may be identified with its protonation (i.e., following proton extraction from either the solvent or the supporting electrolyte); the protonated species would then be responsible for the anodic peak at −0.50 V. Fig. 5 further illustrates the issue.

Here, the CV patterns (Fig. 5a–b) also suggest that, following its oxidation, the protonated flavin undergoes a rather fast deprotonation thus restoring the pristine species. This working hypothesis was confirmed by the digital simulation of the CV curves that was carried out according to the square mechanism depicted in Scheme 4, which includes all pseudo-first order follow-up reactions, see Fig. 5c–d.

Such a mechanism is reminescent of the typical complex reduction behaviour of flavins in protic solvents where, reduced flavins may undergo proton uptake reactions at any redox level (see Scheme 1).

In the present case, because of the expectedly very low free proton content under our experimental conditions and of the

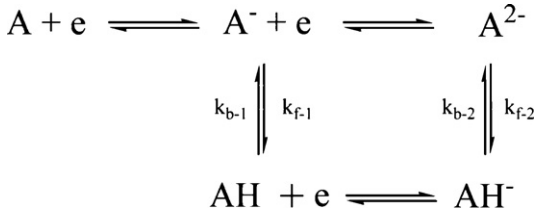

Scheme 4. Square mechanism for flavin-centred electrochemistry. Herein A indicates the relevant flavine moiety in all investigated species and AH its protonated form.

very low acidity of THF, protonation may only have little, though sizeable, effects on the voltammetric behaviour of the investigated species. The simulations were carried out at various scan rates over the range 0.5–50 V s^{-1}. The relevant standard potentials reported in Table 2 and the following kinetic parameters (with 30% uncertainty) were obtained from the simulation: $k_{f\text{-}1} = 5 \times 10^6\ s^{-1}$ $k_{f\text{-}2} = 4 \times 10^2\ s^{-1}$; $k_{b\text{-}1} = 5 \times 10^2\ s^{-1}$, $k_{b\text{-}2} = 4 \times 10^2\ s^{-1}$ for **MF4**, and very similar values were obtained for **MF6**. In conclusion, the CV characterization would then highlight that (i) in all species, the protonation/deprotonation steps of flavin dianions are relatively fast processes, and (ii) sizeable, although minor, electronic interactions between flavin and oxynaphthalene moieties in the macrocycles are likely responsible for the shift of the standard potentials for the first reduction compared to the models. Such an effect was larger in **MF4** than in **MF6** and was not observed in the open forms **OF4** and **OF6**. A small shift of the oxidation potential of the oxynaphthalene moiety was also found in both macrocycles compared to the model species (Table 2), in line with the above-mentioned intercomponent weak interaction. Notice that the opposite effects seem to take place at the level of the second reduction of the flavin moieties in both **MF4** and **MF6**, where a negative shift is observed with respect to the open forms and model. As confirmed by the digital simulation of the voltammetric curves, such a reduction is affected by a larger activation energy than the first one (the corre-

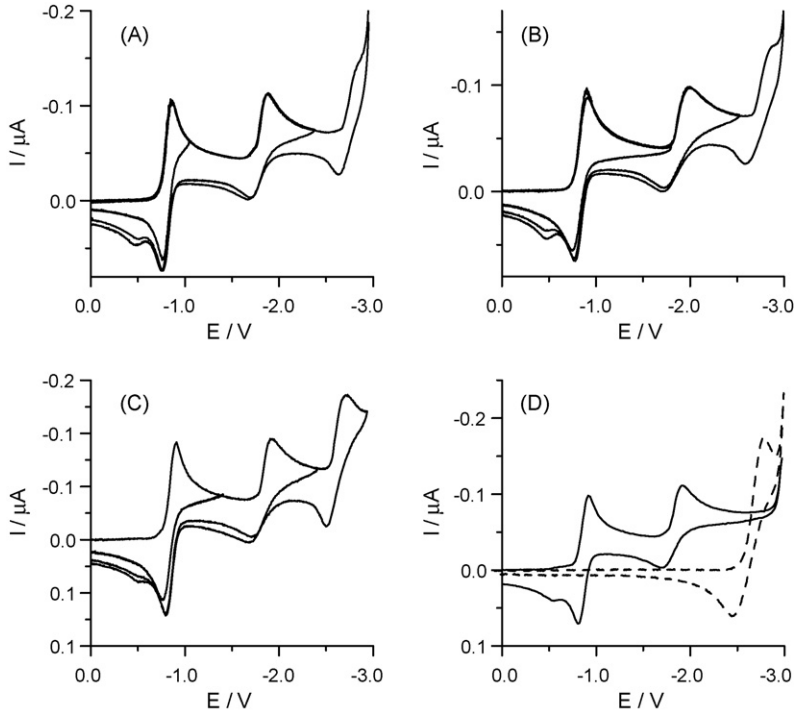

Fig. 4. Cyclic voltammetry curves for a 70 mM TBAH THF solution of (a) 1 mM **MF4**, (b) 1 mM **MF6**; (c) 1 mM **OF4** and (d) 1 mM **FL6** (solid line), 1 mM **dmona** (dotted line). Scan rate: 1 V/s, T = 25 °C. Working electrode: Pt disc (125 μm diameter).

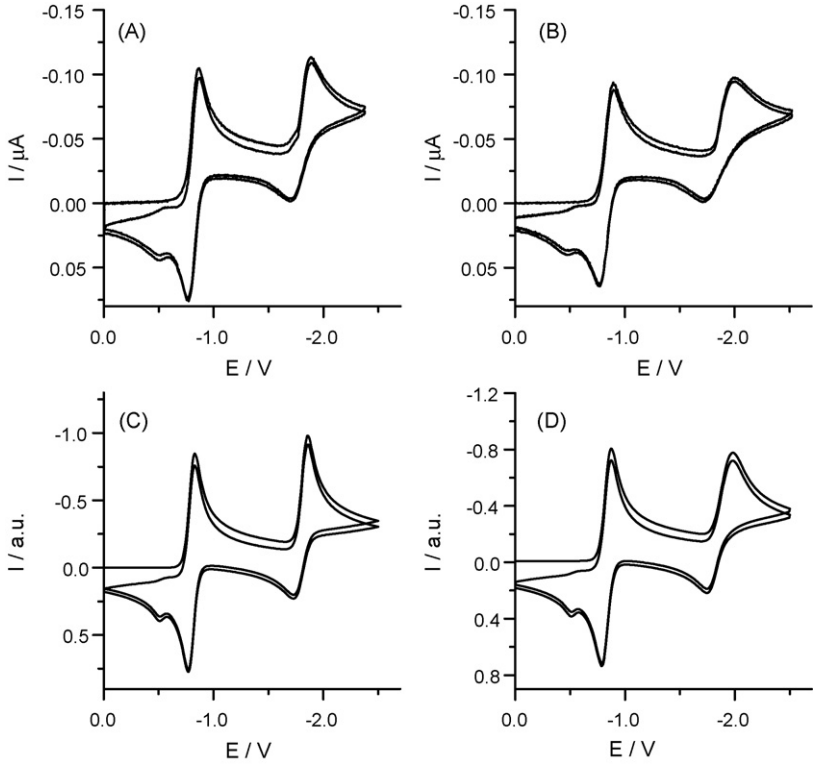

Fig. 5. Cyclic voltammetry curves for a 70 mM TBAH THF solution of (a) 1 mM **MF4**, (b) 1 mM **MF6**. Scan rate: 1 V/s, $T = 25\,^{\circ}C$. Working electrode: Pt disc (125 μm diameter). (c–d) Digitally simulated CV curves of **MF4** (c) or **MF6** (c) calculated according to the mechanism depicted in Scheme 4 under the conditions of a–b.

sponding heterogenous electron transfer rate constants for the two processes, reported in Table 2, differ by about 2 orders of magnitude), and this would likely hinder the effects of any inter-moiety interaction.

3.4. Photophysical measurements

Fig. 6 displays the absorption spectra of the investigated compounds.

Comparison of the absorption properties for the **dmona** (that of **mona** is practically overlapping), **FL6** and bichromophores **OF4**, **OF6**, **MF4**, and **MF6** indicates that for the bichromophores the absorption profile in the visible region is only due to the **FL6** component and the weak absorption at higher energy, peaking at 328 nm, $\varepsilon = 3100\ M^{-1}\ cm^{-1}$, is due to the **ona** components.

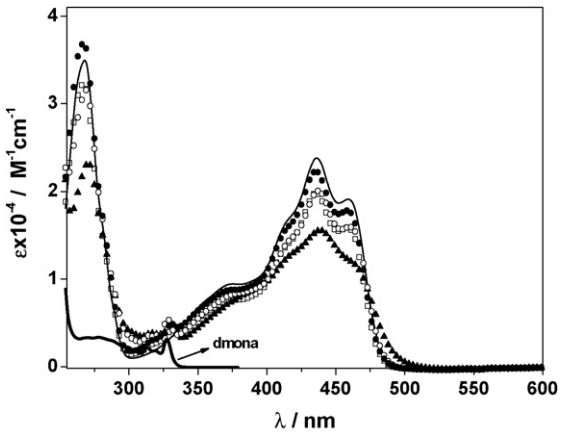

Fig. 6. Room temperature electronic absorption spectra of **OF4** (●), **OF6** (□), **MF4** (▲), **MF6** (○), **FL6** (solid thin line) and **dmona** (solid thick line) in CH_2Cl_2 solution.

All the bichromophores but **MF4** display nearly overlapping profiles indicating that the intercomponent electronic interaction is weak and that the component chromophores practically retain their individual electronic properties. On this basis, for the bichromophores, selected excitation of the **FL6** component can be performed. Accordingly, the luminescence spectra depicted in Fig. 7 were obtained upon excitation of isoabsorbing solutions at 407 nm.

Notably, the luminescence shapes in Fig. 7 exhibit the same band maximum and shape. This indicates that the luminescence can be ascribed to the quenched S_{FL6} level of the **OF**-type moieties (and the same holds for **OF4**, **MF4**, and **MF6**). Table 3 collects luminescence results and derived quenching rate constants, k_{el}, according to Eq. (1), where τ_o and τ_q are the fluorescence lifetimes detected for **FL6**

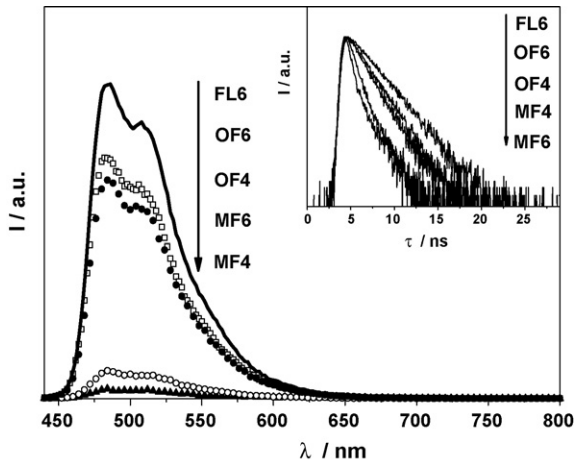

Fig. 7. Room temperature luminescence spectra of the indicated compounds (same symbols as in Fig. 4) as obtained upon excitation of isoabsorbing solutions at 407 nm; solvent is CH_2Cl_2. The inset shows the luminescence decays, $\lambda_{exc} = 407$ nm.

Table 3
Luminescence data and rate constants for intramolecular quenching[a].

	λ_{em} (nm)	ϕ_S	τ_S (ns)	k_{el} (s^{-1})[b]
FL6	483	0.22	2.5	
OF4	483	0.16	1.9	1.3×10^8
OF6	483	0.13	1.7	1.9×10^8
MF4	483	0.01	0.3 (70%)[c] 1.6 (30%)	2.9×10^9[c]
MF6	483	0.02	0.8 (90%)[c] 2.3 (10%)	8.5×10^8[c]

[a] Air-equilibrated CH_2Cl_2 solvent, room temperature, λ_{exc} = 407 nm for both spectra and lifetimes.
[b] According to Eq. (1) and concerned text.
[c] Results obtained according to a dual exponential analysis; actually, the time dependent behaviour of the emission is likely related to a complex distribution of conformers, and evaluation of the quenching constant is only performed for the major component.

and the bichromophores, respectively.

$$k_{el} = \frac{1}{\tau_q} - \frac{1}{\tau_o} \quad (1)$$

Such k_{el} values were interpreted as the rate constants of the corresponding **FL6*** ← **ona** electron transfer steps. As a matter of fact, the potentially competing deactivation paths by either $S_{\mathbf{FL6}} \rightarrow S_{\mathbf{ona}}$ or $S_{\mathbf{FL6}} \rightarrow T_{\mathbf{ona}}$ intramolecular energy transfer processes resulted in both cases energetically prohibited: from Fig. 7, the energy content of the $S_{\mathbf{FL6}}$ level is 2.6 eV while $S_{\mathbf{ona}}$ lies at >3.8 eV [6,7] and $T_{\mathbf{ona}}$ at 2.6 eV (i.e., isoergonic of $S_{\mathbf{FL6}}$). On the other hand, a favourable driving force $\Delta G^\circ \cong -0.3$ eV for **FL6*** ← **ona** electron transfer was estimated by using Eq. (2) and the standard potentials reported in Table 2.

$$\Delta G^\circ \cong e \cdot (E^{ox}_{1/2} - E^{red}_{1/2}) - E_S \quad (2)$$

Further details on the evaluation of **FL6** → **ona** energy transfer steps are reported in the SI.

In Fig. 8, 10 μs-delayed luminescence spectra for **FL6** and **OF6** as observed at 77 K (i.e., in glassy solution) are compared upon excitation with λ = 407 nm. As seen above, in both cases at this wavelength, the $S_{\mathbf{FL6}}$ level is initially populated. For **OF6** in frozen solvent the photoinduced electron transfer step should be inhibited because not enough exothermic [27], and the observed profile is attributed to a phosphorescent level. The fact that the spectra of both **FL6** and **OF6** exhibit the same shape and peak maximum, supports the notion that the lowest-lying level in the bichromophore is of $T_{\mathbf{FL6}}$ nature, lying at ca. 2.14 eV (as drawn from the band maximum in Fig. 8). It should further be noticed that also at room temperature, for **OF6** and for the other bichromophores examined here, no photoinduced electron transfer can take place upon involvement of the $T_{\mathbf{FL6}}$ level. Actually, its energy content $E_T \sim 2.14$ eV is not large enough to render exothermic the $T_{\mathbf{FL6}}$ ← **ona** electron transfer step, Eq. (2) upon replacement of E_S by E_T.

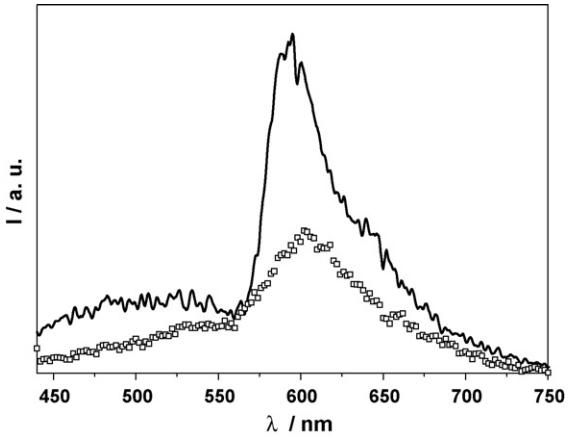

Fig. 8. Time-delayed (10 μs) luminescence spectra observed at 77 K for **FL6** (solid line) and **OF6** (□); λ_{exc} = 407 nm, solvent CH_2Cl_2.

4. Conclusions

Cyclic voltammetric experiments performed under strictly aprotic conditions evidenced sizeable shifts of the redox potentials of both flavin reduction and oxy-naphthalene oxidation in the macrocyclic bichromophores that were instead absent in the corresponding open forms. This suggested a significant role played by the relative position of the two moieties for the occurrence of the mutual inter-moiety interaction. As a matter of fact, photoinduced electron transfer processes were found to take place between the two moieties that were significantly faster in the closed macrocyclic bichromophores than in the corresponding open forms. The present study opens the way to a new family of electroactive–photoactive molecular architectures containing lumiflavins and other electroactive aromatic rings such as anthraquinones and naphtoquinones capable to recognise, e.g., biogenic amines such as dopamine. Work on new macrocyclic hosts based on the ones discussed in this paper is currently underway.

Acknowledgements

This work was supported by the Spanish Science and Education Ministry (MEC), CTQ2007-62113 and by the University of Bologna. M.A. Farrán is indebted to the Former Spanish Ministry of Science and Technology for a Ramón y Cajal Research Contract. We would like to thank Professor Wolfgang Holzer and Dr. Gernot Eller (University of Vienna) for their help providing the IUPAC names for compounds **MF4** and **MF6**. Prof. D. Sanz del Castillo is acknowledged for her help performing the NOE experiments.

Appendix A. Supplementary data

Supplementary data associated with this article can be found, in the online version, at doi:10.1016/j.jphotochem.2009.01.012.

References

[1] P.F. Heelis, Chem. Soc. Rev. 11 (1982) 15.
[2] C.W.M. Kay, A. Kuppig, E. Schleicher, A. Bacher, G. Richter, S. Weber, Blue light-induced DNA repair by photolyase, in: E. Silva, A.M. Edwards (Eds.), Comprehensive Series in Photochemical and Photobiological Sciences, D. Häder and Jori, 151, Cambridge, UK, 2006.
[3] W.M. Moore, R.C. Ireton, Photochem. Photobiol. 25 (1977) 347.
[4] J.J. Hasford, C.J. Rizzo, J. Am. Chem. Soc. 120 (1998) 2251.
[5] Y.J. Zheng, R.L. Ornstein, J. Am. Chem. Soc. 118 (1996) 9402.
[6] T.C. Bruice, T.W. Chan, J.P. Taulane, I. Yokoe, D.L. Elliott, R.F. Williams, M. Novak, J. Am. Chem. Soc. 99 (1977) 6713.
[7] S.O. Mansoorabadi, C.J. Thibodeaux, H.W. Liu, J. Org. Chem. 72 (2007) 6329.
[8] A. Niemz, V.M. Rotello, Accounts Chem. Res. 32 (1999) 44.
[9] E.C. Breinlinger, V.M. Rotello, J. Am. Chem. Soc. 119 (1997) 1165.
[10] R.M.G. Hynson, S.M. Kelly, N.C. Price, R.R. Ramsay, Biochim. Biophys. Acta-Gen. Subj. 1672 (2004) 60.
[11] K. Sadeghian, M. Schutz, J. Am. Chem. Soc. 129 (2007) 4068.
[12] P.R. Callis, T.Q. Liu, Chem. Phys. 326 (2006) 230.
[13] F. Bosca, L. Fernandez, P.F. Heelis, Y. Yano, J. Photochem. Photobiol. B-Biol. 55 (2000) 183.
[14] F. Tanaka, H. Chosrowjan, S. Taniguchi, N. Mataga, K. Sato, Y. Nishina, K. Shiga, J. Phys. Chem. B 111 (2007) 5694.
[15] P. Mattei, F. Diederich, Angew. Chem. -Int. Ed. Engl. 35 (1996) 1341.
[16] E.M. Seward, R.B. Hopkins, W. Sauerer, S.W. Tam, F. Diederich, J. Am. Chem. Soc. 112 (1990) 1783.
[17] S. Shinkai, A. Kawase, T. Yamaguchi, O. Manabe, Y. Wada, F. Yoneda, Y. Ohta, K. Nishimoto, J. Am. Chem. Soc. 111 (1989) 4928.
[18] H.A. Staab, M.F. Zipplies, T. Muller, M. Storch, C. Krieger, Chem. Berichte 127 (1994) 1667.

[19] G. Porcal, S.G. Bertolotti, C.M. Previtali, M.V. Encinas, Phys. Chem. Chem. Phys. 5 (2003) 4123.
[20] M. Montalti, A. Credi, L. Prodi, M.T. Gandolfi, Handbook of Photochemistry, third ed., CRC Press, Taylor & Francis, Boca Raton, 2006.
[21] R.M. Kowalczyk, E. Schleicher, R. Bittl, S. Weber, J. Am. Chem. Soc. 126 (2004) 11393.
[22] E. Sikorska, I.V. Khmelinskii, D.R. Worrall, J. Koput, M. Sikorski, J. Fluorescence 14 (2004) 57.
[23] Z. Shen, R. Prochazka, J. Daub, N. Fritz, N. Acar, S. Schneider, Phys. Chem. Chem. Phys. 5 (2003) 3257.
[24] J. Shirdel, A. Pertzkofer, Z. Shen, R. Prochazka, J. Daub, Chem. Phys. 337 (2007) 99.
[25] A. Farrán, R.M. Claramunt, C. Lopez, E. Pinilla, M.R. Torres, J. Elguero, Arkivoc (2007) 20.
[26] F. Yoneda, Y. Sakuma, M. Ichiba, K. Shinomura, J. Am. Chem. Soc. 98 (1976) 830.
[27] G.L. Gaines, M.P. Oneil, W.A. Svec, M.P. Niemczyk, M.R. Wasielewski, J. Am. Chem. Soc. 113 (1991) 719.
[28] J.N. Demas, G.A. Crosby, J. Phys. Chem. 75 (1971) 991.
[29] K. Nakamaru, Bull. Chem. Soc. Jpn. 55 (1982) 2697.
[30] (a) A.A. La Pensée, J. Bickley, S.J. Higgins, M. Marcaccio, F. Paolucci, S. Roffia, J.M. Charnock, J. Chem. Soc., Dalton Trans. (2002) 4095;
(b) F. Cecchet, A.M. Gioacchini, M. Marcaccio, F. Paolucci, S. Roffia, M. Alebbi, C.A. Bignozzi, J. Phys. Chem. B 106 (2002) 3926.
[31] S. Cattarin, P. Ceroni, D.M. Guldi, M. Maggini, E. Menna, F. Paolucci, S. Roffia, G. Scorrano, J. Mater. Chem. 9 (1999) 2743.
[32] C. Amatore, C.J. Lefrou, Electroanal. Chem. 324 (1992) 33.
[33] Antigona developed by Dr. Loïc Mottier, University of Bologna, Bologna, Italy, 1999.
[34] G.M. Sheldrick, Programme for Refinement of Crystal Structure, University of Gottingen, 1997.
[35] A.L. Spek, Acta Cryst. A46 (1990), C-34.